nature photonics

LETTERS

PUBLISHED ONLINE: 24 JUNE 2012 | DOI: 10.1038/NPHOTON.2012.126

Fluctuations and correlations in modulation instability

D. R. Solli[1,2]*, G. Herink[2], B. Jalali[1,3] and C. Ropers[1,2]

Stochastically driven nonlinear processes are responsible for spontaneous pattern formation and instabilities in numerous natural and artificial systems, including well-known examples such as sand ripples, cloud formations, water waves, animal pigmentation and heart rhythms[1–3]. Technologically, a type of such self-amplification drives free-electron lasers[4,5] and optical supercontinuum sources[6,7] whose radiation qualities, however, suffer from the stochastic origins[8–11]. Through time-resolved observations, we identify intrinsic properties of these fluctuations that are hidden in ensemble measurements. We acquire single-shot spectra of modulation instability produced by laser pulses in glass fibre at megahertz real-time capture rates. The temporally confined nature of the gain physically limits the number of amplified modes, which form an anti-bunched arrangement as identified from a statistical analysis of the data. These dynamics provide an example of pattern competition and interaction in confined nonlinear systems.

Nonlinear dynamics arising in fluids[3], plasmas[12], discrete lattices[13], ultracold quantum gases[14,15], free-electron lasers[4,5], optics[6,16,17] and other systems can cause the spontaneous growth of temporal or spatial oscillations that are nearly absent in the initial conditions. Termed modulation instability, this nonlinear action leads to pattern formation from stochastic fluctuations in a wide variety of systems and has recently been described as 'one of most ubiquitous types of instabilities in nature'[18]. As a quintessential example of stochastically driven nonlinear dynamics, studies of this phenomenon (and the associated occurrence of solitary waves) rapidly spread into different branches of physics from the 1960s[18] onwards, revealing strikingly similar characteristics in many situations. For example, sand ripples and dunes[2], water wave instabilities[3,19,20], matter–wave pulses[14,15] and nonlinear oscillations in optics[6,21] exhibit many of the same features, although the underlying physical mechanisms are of course quite different. Common experience suggests that such processes usually favour growth at a single frequency: different waves amplified by modulation instability tend to avoid direct overlap or beating with each other in the same spatial or temporal domain. The emergence of a quasi-monochromatic modulation from a broadband (white) noise background implies complex dynamics of mode interaction and competition.

Here, we observe the spontaneous appearance of discrete frequency modes in a real-time experimental investigation of pulsed modulation instability in an optical system. We find direct evidence of a competitive mode interaction, which becomes observable by a statistical analysis of many single-shot spectra. Specifically, a number of key aspects are apparent in this pulsed (that is, temporally-confined) situation: modulation instability amplifies discrete spectro-temporal features, displays Stokes/anti-Stokes mode asymmetry and exhibits prominent mode competition. These features dominate the dynamics when the duration of the time-limited domain becomes comparable to the coherent extension of the individual modes, but are normally unrecognizable due to inhomogeneous broadening of the modulation instability gain profile. The mode interaction favours a 'winner takes all' scenario and shows how single patterns may come to dominate a given spatial or temporal region.

Modulation instability is typically excited with a continuous or quasi-continuous wave and observed in a time-averaged manner[6]. In this direction, breather solutions and Fermi–Pasta–Ulam recurrences have attracted interest in fluid dynamics and optics[22–25]. Continuous-wave conditions, which correspond to an effectively unbounded modulation instability domain, yield information on the general tendencies for instability and average behaviour of the nonlinear process, but usually prevent a time-resolved view of the stochastic dynamics. Other important research has shown that modulation instability occurs with incoherent excitation and a non-instantaneous nonlinearity for a threshold power level[17]. In such situations, uncorrelated regions of an incoherent driving wave act in concert rather than as a collection of independent domains. In contrast, the present study harnesses an instantaneous nonlinearity and examines the impact of confinement on modulation instability; the collection of a large volume of single-shot spectra facilitates a 'microscopic' investigation of the instability and associated pattern interaction.

In technology, pulse-driven modulation instability is crucial in the generation of an ultra-broadband supercontinuum from narrowband input light[7]. This form of white light is becoming increasingly prevalent in imaging and spectroscopy and is available using compact commercial instruments, which harness the instability and the associated soliton fission[26,27]. Modulation instability also drives light generation in self-amplified spontaneous-emission (SASE) free-electron lasers. Radiation generated by an undulating high-energy electron bunch acts back on the bunch, leading to further modulation of the electron distribution and to radiation build-up[4]. In both supercontinuum generation and SASE free-electron lasing, the initiation of modulation normally arises spontaneously from noise, translating to shot-to-shot spectral variations in the output radiation and loss of temporal coherence[8,9]. Recent experiments in optics have shown that even unusual rare events—optical rogue waves—can be generated in this process[21]. However, in both supercontinuum generation and free-electron lasing, coherent seeding of modulation instability can be used to stabilize and manipulate the output field[4,28–30].

In our experiments, a stream of mode-locked picosecond light pulses (wavelength, 1,550 nm; repetition rate, 25 MHz; duration, ~3 ps) are injected into highly nonlinear single-mode fibre (near its zero-dispersion wavelength) to produce spontaneous modulation instability (Fig. 1). The output light is linearly stretched in a spool of dispersive fibre (large normal dispersion) so that the optical spectrum of each pulse can be captured in real time by a photodetector and a real-time oscilloscope[31]. This crucial step allows

[1]Department of Electrical Engineering, University of California, Los Angeles, California 90095, USA, [2]Courant Research Center Physics and Materials Physics Institute, University of Göttingen, Germany, [3]California NanoSystems Institute (CNSI), Los Angeles, California 90095, USA. *e-mail: solli@ucla.edu

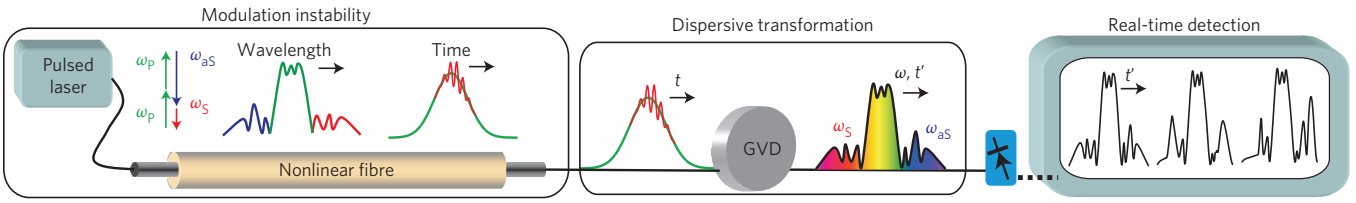

Figure 1 | Capturing modulation instability in single-shot measurements. Laser pulses spontaneously induce modulation instability in nonlinear fibre. Annihilation of two input (pump, ω_p) photons yields one redshifted (Stokes, ω_S) photon and one blue-shifted (anti-Stokes, ω_{aS}) photon. The Stokes and anti-Stokes components appear as sidebands around the input spectrum (envelope modulation in the time domain). Because of their stochastic origins, these components fluctuate from pulse to pulse. To resolve the single-shot properties of modulation instability, the output pulses are subjected to substantial group-velocity dispersion (GVD), which maps frequency into time and stretches the temporal scale[31] so that thousands of individual spectra can be acquired in real time (megahertz capture rates) with a photodiode and a real-time oscilloscope.

pulse-resolved spectral measurement with subnanometre resolution at the full laser repetition rate, rather than averaging over many pulses with a conventional spectrometer. In this manner, many thousands of spectra from consecutive single laser pulses are collected and analysed statistically.

Figure 2a,b presents a selection of measured single-shot spectra for two different pump power levels, together with time-averaged spectra (for additional spectra see Supplementary Fig. S1). The spectra contain a spectrally broadened central pump peak (due to self-phase modulation, SPM[6]) and adjacent features stemming from modulation instability, corresponding to frequency-downshifted (Stokes) and upshifted (anti-Stokes) portions. It is apparent that the single-shot spectra consist of discrete, sharp features whose widths, amplitudes and positions vary drastically from pulse to pulse because they are initiated by optical noise overlapping with the modulation instability gain. The number of peaks per spectrum displays equally strong variations, with some pulses exhibiting multiple peaks and others showing essentially no sign of modulation instability at all. These latent spectral features wash out to the known smooth modulation instability sidebands in the average spectrum. We note that pump power fluctuations from the mode-locked laser are miniscule (<0.1%, estimated from radio-frequency spectral measurements) and not the cause of these observations. Fluctuations of the central SPM-broadened pump arise from pump depletion connected to the variations in modulation instability. Structured profiles are also known to arise in the single-shot spectra of free-electron lasers[8,9], underscoring the similarities of time-limited modulation instability in different contexts and suggesting that these findings have broad applicability.

Notably, most single-shot spectra do not exhibit Stokes/anti-Stokes mirror symmetry. This may be surprising in light of a four-wave mixing description in which two degenerate pump photons are converted symmetrically into Stokes and anti-Stokes photons. Indeed, the time-averaged spectrum at low pump power (Fig. 2a, top trace) does not show such asymmetries. Figure 2c compares the Stokes and anti-Stokes peak spectral densities for 5,000 events at this power level and shows that a correlation rapidly diminishes beyond low levels of modulation instability. Modulation instability symmetry breaking is known to occur from higher-order dispersion[32,33], Raman scattering and early soliton formation[6,7]. Although such effects are visible in time-averaged measurements, the prominent asymmetries in the time-resolved spectra at low to moderate pump power arise primarily from a different source: SPM-induced broadening of the pump field generates an expanding range of pump wavelengths that can participate in elementary four-wave mixing processes. These varied frequency combinations lead to many asymmetric outcomes in the single-shot spectra, but the asymmetry largely disappears with ensemble averaging. At higher power levels and/or large modulation instability amplitudes, early soliton formation and Raman scattering begin to play a role, adding more weight to the Stokes region, as seen in both the single-shot and time-averaged spectra. Overall, it is evident that single-shot spectroscopy reveals forms of asymmetry hidden by averaging.

The usual picture of modulation instability encompasses a gain bandwidth that describes the range of wavelengths over which gain exists. Based on the present data, it becomes clear that this bandwidth should be viewed as an *inhomogeneously* broadened quantity, whereas the intrinsic (*homogeneous*) lines are in fact much narrower. The homogeneous linewidth has a lower limit from the temporal confinement of the modulation instability gain window, which restricts the coherence time of any amplified feature. Features exist with a continuum of amplitudes; the typical mode population depends on pump power and scales approximately with the ratio of the inhomogeneous to homogeneous bandwidths.

The duration of the pump pulse sets a coarse upper limit to the coherence time. In the present case, this suggests a mode linewidth as small as ~0.3 THz. However, the typical widths seen in the single-shot data are somewhat broader, indicating that the temporal gain window is actually a few times shorter than the pump envelope. This restricted coherence time is set by the nonlinear phase-matching requirement (momentum conservation) between the Stokes, anti-Stokes and pump fields, where the latter has been chirped by SPM (see Supplementary Information). In short, there is a limited time interval over which phase matching can be maintained for a given modulation instability feature because the pump frequency varies across the envelope. The mode diversity arises from applying this gain window to the noise profile. Transform-limited modes are phase matched for a relatively short time, whereas chirped modes tracking the pump can be amplified for a longer period.

Numerous properties can be extracted from the data by sorting peaks based on various criteria. For example, Fig. 2d shows the dependence of the homogeneous linewidth on peak amplitude for several different power levels. The linewidth tends to decrease with increasing pump power and, at constant power, the stronger peaks are also generally the narrowest. Such a narrowing effect is a universal property of gain processes, but is not observed in time-averaged measurements of stochastically driven optical modulation instability. Instead, time-averaged measurements can only detect the range of instability, which is known to increase with power[6]. We also find that the smallest features tend to experience initial broadening (Fig. 2d) due to the confinement; if the initial mode extension is longer than the temporal gain slot, windowing broadens the mode before gain narrowing dominates.

The time-limited excitation restricts the number of amplified modes and ensures that they are in relatively close temporal proximity. These conditions favour the identification of mode interaction, which can be investigated with a statistical analysis of intra-pulse spectral correlations in a large population of single-shot spectra. Here, this information is extracted directly from the raw data by applying a type of autocorrelation analysis suited for inhomogeneously broadened spectra. The approach we employ was

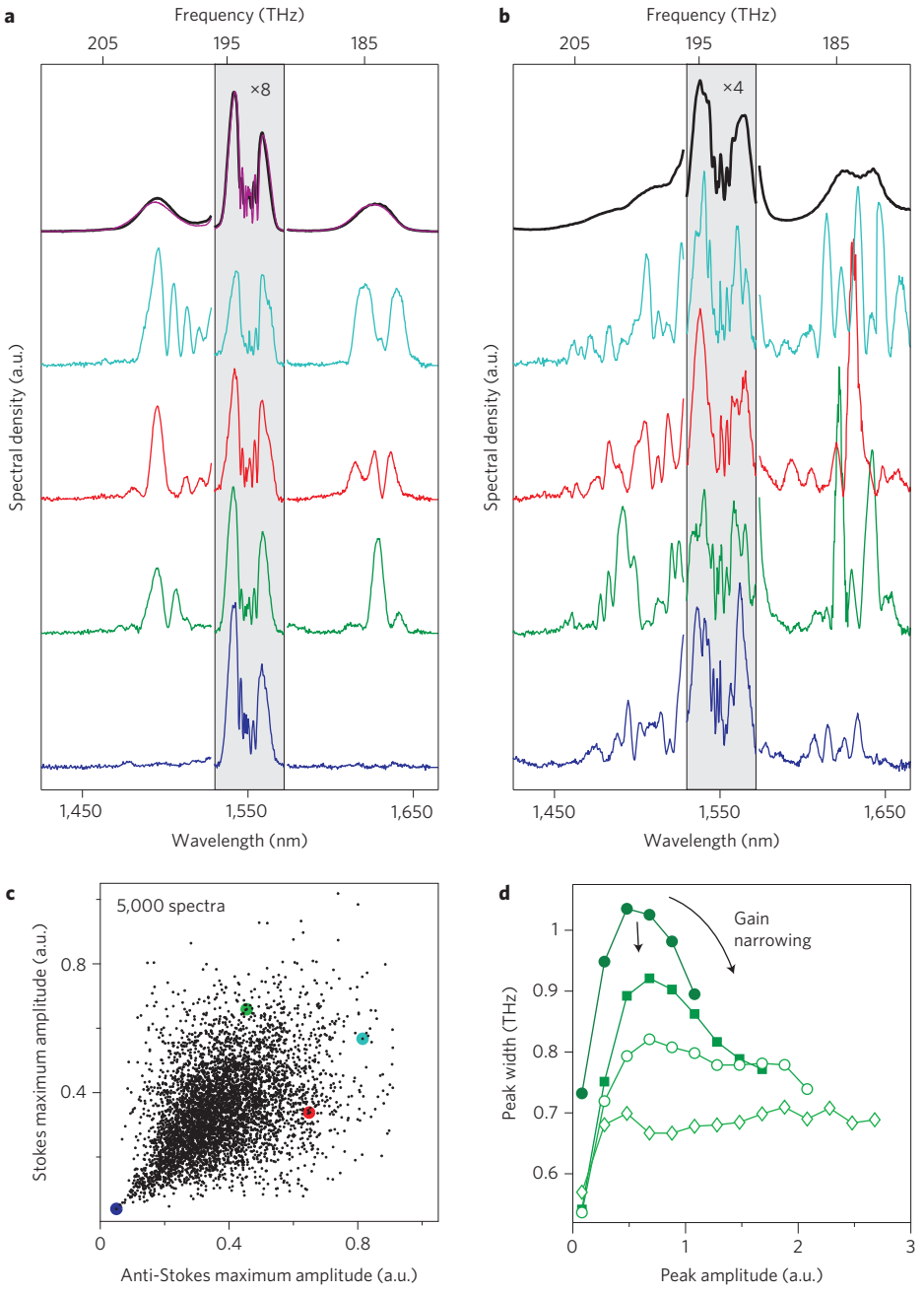

Figure 2 | Experimental investigation of single-shot modulation instability. a,**b**, Selected single-shot spectra (coloured traces) obtained with low (**a**, 80 W) and higher (**b**, 100 W) input power. Top traces (black) are the averages of 5,000 single-shot spectra at the two power levels. For comparison, a time-averaged measurement with a conventional optical spectrum analyser is overlaid on the top curve in **a** (purple), showing very good agreement. The central portions (grey shading) are vertically scaled (multiply by the indicated factor for actual size) to facilitate viewing of the broadened input and modulation instability features. **c**, Scatter plot of the peak power spectral density of Stokes and anti-Stokes components for 5,000 spectra (80 W input); coloured dots indicate the events for the corresponding coloured spectra in **a**. **d**, Stokes modulation instability peak width versus peak amplitude at four different input power levels (top to bottom: 80 W, 85 W, 90 W, 100 W). Arrows indicate gain narrowing across different input power levels and for larger peaks. Anti-Stokes trends are shown in Supplementary Fig. S2.

previously used to identify quantum-mechanical level repulsion in nanostructure photoluminescence[34]. It is sensitive to those correlations that are present in the individual spectra and removes the background from the overall spectral shape. The background-free correlation function is obtained by forming the average of the spectral autocorrelations $\langle S_n \star S_n \rangle$ of all single-shot experimental spectra S_n and subtracting the autocorrelation of the averaged spectrum $\langle S_n \rangle \star \langle S_n \rangle$. Simply put, we compute the average autocorrelation minus the autocorrelation of the average. Figure 3 presents the results of this analysis for the Stokes and anti-Stokes modulation instability regions at three different power levels as a function of frequency shift, together with examples of the two parent quantities.

The correlation functions display a positive central peak at zero frequency shift and a negative valley of varying depth and width (shaded regions). The central peak arises from the fact that all individual spectra consist of narrow lines that are absent in the average spectrum, whereas the features at larger frequency shift originate from the interaction between different lines. (Note that spectral

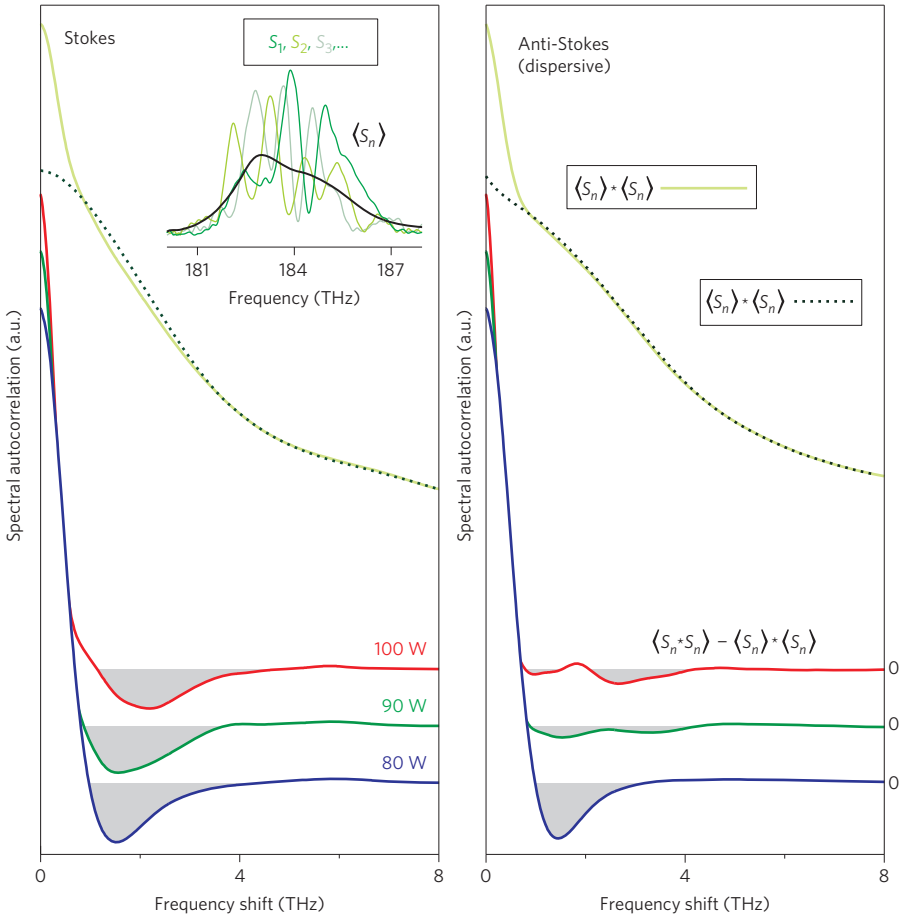

Figure 3 | Autocorrelation analysis of experimental single-shot modulation instability spectra. A background-free autocorrelation function for the Stokes (left) and anti-Stokes (right) modulation instability features is obtained by forming the average of the spectral autocorrelations $\langle S_n * S_n \rangle$ of 5,000 single-shot spectra S_n and subtracting the autocorrelation of their average $\langle S_n \rangle * \langle S_n \rangle$. The function is computed from experimental data at three different input power levels (80 W, 90 W, 100 W), and example parent functions $\langle S_n * S_n \rangle$ and $\langle S_n \rangle * \langle S_n \rangle$ are shown for 90 W input. Inset: single-shot spectra and average spectrum for the Stokes portion at this power level.

jitter can in principle also lead to negative features in such an analysis; here, however, it does not play a significant role and would generally also produce much broader depressions.) If the separate peaks were uncorrelated, the analysis would yield only a central peak on a flat background because each feature would only be correlated with itself. In turn, negative values signify the fact that such peak spacings are underrepresented in the individual events (anti-correlation). The experimental data for the Stokes lines show a persistent anti-correlation that changes subtly with power, but it diminishes with increasing power on the anti-Stokes side. It should be noted that the anti-Stokes spectral region is dispersive, whereas the Stokes band supports soliton formation. The difference may account for the observed reduction in anti-Stokes mode correlations at high power levels. In quantum optics, correlations *between* Stokes and anti-Stokes photons (arising from energy conservation) are often considered[35]; here, we find correlations at the single-shot level *within* the Stokes and anti-Stokes bands individually.

The present results show that modulation instability is an interactive gain process, resulting in a preferred frequency spacing between modes. Although the origin of this interaction may have multiple facets, one mechanism is described here. Two developing modulation instability features will interact to produce a temporal beating on the pump pulse envelope if the features are in close spectral proximity (within a characteristic range of influence). Even at the earliest stages of the development of modulation instability, this interference will influence and couple their individual gains. Depending on the frequency separation and relative phase of the modes, the interference will be either constructive or destructive near the centre of the temporal gain window. We find that both of these limiting cases lead to a reduced occurrence of closely spaced gain features (Supplementary Fig. S5). Destructive interference produces a beating with a null in the middle of the gain window, reducing the gain for both features (suppression). On the other hand, constructive interference causes the gain features to merge in the nonlinear propagation because the temporal confinement and bandwidth-restricted gain damp out the beating. Together with gain narrowing, this creates an attractive effect, which again reduces the likelihood of closely spaced separate peaks and broad features.

To investigate whether the existing theoretical framework for modelling modulation instability can account for the observed spectral features and correlations, we perform numerical simulations using the generalized nonlinear Schrödinger equation (NLSE). The NLSE is known to be effective in modelling spectral and temporal effects of nonlinear propagation in fibre[6,7], but the mode structure and correlations shown here have not been studied previously. In the simulations, input noise is included to account for the stochastic variations and its amplitude is adjusted to produce the amount of time-averaged modulation instability gain seen in the experiment. To compare individual single-shot spectra with the experimental results, we perform ~1,000 independent simulations at a fixed input power level, and indeed identify very

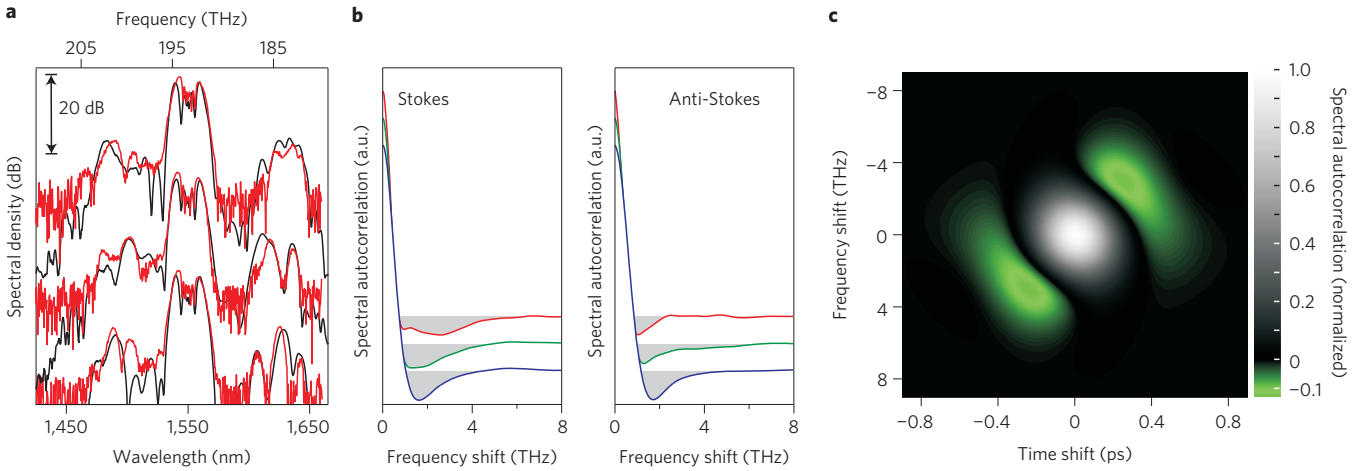

Figure 4 | Analysis of modulation instability in nonlinear optical fibre by numerical simulation. a, Selected single-shot simulated (black) and experimental (red) spectra. Similar simulated and experimental spectra are found by comparing the Stokes overlap. **b**, Spectral autocorrelation functions computed from 1,000 simulated single-shot spectra for Stokes (left) and anti-Stokes (right) modulation instability. Input power levels: 80 W (blue), 90 W (green), 100 W (red). **c**, Two-dimensional version of the spectral autocorrelation function for Stokes modulation instability computed from 1,000 simulated events (80 W input). Negative values (green regions) indicate underrepresented time/frequency spacings in the events, indicating an anti-correlation of modulation instability gain features in both the spectral and temporal domains.

similar single-shot features. Striking correspondences can be found by postselecting events that are similar to those observed in the experiment (Fig. 4a).

The correlation analysis can now equally be applied to the simulated spectra (Fig. 4b). We find that the spectral correlations in the simulations and experiments are very similar, with some discrepancies for the anti-Stokes at high power. Given the complexity of the dynamics and its sensitivity to multiple experimental parameters, including higher-order dispersion and polarization, the agreement is quite remarkable and suggests that the correlations found are a general property of modulation instability. We note that the existence of correlations does not require a specific input noise level and occurs in nascent modulation instability. The close correspondence between simulation and experiment gives confidence that the analysis can be analogously extended to the temporal domain in the simulations, or to time–frequency spectrograms (Supplementary Figs S3,S4). In essence, the correlation method is applied to windowed Fourier transforms or spectrograms (gate, 250 fs) of 1,000 simulated events, where both frequency and temporal shifts become arguments of the correlation function. This analysis shows that the anti-correlation exists in both frequency and time, being strongest along a linear combination of the two variables (Fig. 4c). The temporal anti-correlation can be understood as a direct extension of previous arguments: the finite gain–bandwidth of modulation instability makes certain spectral beatings less likely, just as confinement in time selects against particular temporal beatings. It can also be explained by noting that the time and frequency domains are coupled through the nonlinear interaction, which causes a correlation in one domain to manifest in the other.

In conclusion, the time-limited properties of modulation instability have been investigated, revealing discrete pulse-like features that maintain an anti-bunched arrangement in both the spectral and temporal domains. The results indicate that the range of frequency components that can be amplified by modulation instability within a limited interval is restricted, a property that may influence emergent spectral and temporal effects such as soliton dynamics and the formation of rare events. We have found that an important factor in the mode interaction originates from the coupling of the modulation instability spectral profile with the temporal gain confinement. The mode interactions are reminiscent of phase-dependent attraction and repulsion in temporal soliton dynamics, but here originate from confinement and appear even for small feature amplitudes. Similar anti-bunching effects will occur in spatial modulation instability, leading to restrictions on the spatial patterns that can spontaneously arise in such systems. These properties are, therefore, expected to influence modulation instability-induced characteristics and those of other parametric processes in a broad range of physical situations and technological systems including free-electron lasers.

Methods

To investigate the time-limited properties of modulation instability, pulses are obtained from a mode-locked laser (1,550 nm; repetition rate, 25 MHz; duration, ~3 ps), amplified in a large-mode-area erbium-doped fibre amplifier, filtered to remove excess amplified stimulated emission, and injected into a 15 m segment of highly nonlinear single-mode fibre. The output light is linearly dispersed in a spool of standard dispersion-compensating fibre (dispersion, −100 ps nm^{-1}) to achieve a dispersive Fourier transform. The dispersed light is split into components that are separately attenuated by different amounts before photodetection and measurement with separate channels of a real-time oscilloscope (operating at 25 GSa s^{-1}). The spectral resolution is ≤1 nm, limited by the photodetector bandwidth (~10 GHz). (A discussion of limiting factors can be found in ref. 36.) Splitting the fibre output allows the pump and modulation instability spectral regions of the signal to be differentially attenuated to increase the effective dynamic range of the single-shot detection system, avoiding photodetector saturation while maximizing signal-to-noise on the oscilloscope. Different portions of the signal from each channel are then digitally combined, achieving a dynamic range of ~25 dB. To calibrate the wavelength scale of the spectrum (~1,410–1,670 nm), many single-shot spectra are averaged and compared with a time-averaged measurement from an optical spectrum analyser.

The simulations of modulation instability are conducted with the generalized NLSE[6,7]:

$$\frac{\partial A(z,t)}{\partial z} = i\sum_{m\geq 2}\frac{i^m\beta_m}{m!}\frac{\partial A(z,t)}{\partial t} + i\gamma\left(1+\frac{i}{\omega_0}\frac{\partial}{\partial t}\right)A(z,t)\int_{-\infty}^{t} R(t')\left|A(z,t-t')\right|^2 \mathrm{d}t'$$

where $A(z,t)$ is the slowly varying field envelope, dispersion is included through coefficients $\beta_2 = 1.13\times10^{-28}$ s^2 m^{-1}, $\beta_3 = 6.17\times10^{-41}$ s^3 m^{-1} and $\beta_4 = -2.07\times10^{-55}$ s^4 m^{-1}, $\gamma = 10.66$ W^{-1} km^{-1} is the nonlinear coefficient, ω_0 is the central wavelength and $R(t) = (1-f_R)\delta(t) + f_R h(t)$ accounts for the instantaneous and Raman responses of the fibre ($f_R = 0.18$). The zero-dispersion wavelength occurs at ~1,552 nm, close to the pump centre. Raman scattering typically does not have a significant impact until relatively late in the fibre unless the input power is large. In the literature, modulation instability is typically seeded by adding phase noise to the input field in the frequency domain with a power amplitude of one photon per mode (per duration of the time window), corresponding to shot noise. Comparing simulations with the present experimental data illustrates that the noise level needed

to model typical experiments is substantially higher, probably because of ASE from the laser and amplifier. We empirically find that bandwidth-limited input noise (Gaussian-shaped, centred at ~1,485 nm, width of ~45 nm, 50 times one-photon-per-mode level at peak) accounts for the modulation instability profile more accurately. In general, the noise characteristics should be left as adjustable parameters because they are not typically precisely known, experimentally. The correspondences seen in Fig. 4a suggest that the input noise profiles from individual measured single-shot spectra can be identified.

Received 4 January 2012; accepted 23 April 2012; published online 24 June 2012

References

1. Cross, M. C. & Hohenberg, P. C. Pattern formation outside of equilibrium. *Rev. Mod. Phys.* **65,** 851–1112 (1993).
2. Elbelrhiti, H., Claudin, P. & Andreotti, B. Field evidence for surface-wave-induced instability of sand dunes. *Nature* **437,** 720–723 (2005).
3. Benjamin, T. B. & Feir, J. E. The disintegration of wave trains on deep water. Part 1. Theory. *J. Fluid Mech.* **27,** 417–430 (1967).
4. McNeil, B. W. J. & Thompson, N. R. X-ray free-electron lasers. *Nature Photon.* **4,** 814–821 (2010).
5. Bonifacio, R., Pellegrinia, C. & Narducci, L. M. Collective instabilities and high-gain regime in a free electron laser. *Opt. Commun.* **50,** 373–378 (1984).
6. Agrawal, G. P. *Nonlinear Fiber Optics* 4th edn (Academic Press, 2007).
7. Dudley, J. M., Genty, G. & Coen, S. Supercontinuum generation in photonic crystal fiber. *Rev. Mod. Phys.* **78,** 1135–1184 (2006).
8. Wellhöfer, M. *et al*. Photoelectron spectroscopy as a non-invasive method to monitor SASE-FEL spectra. *J. Instrum.* **3,** P02003 (2008).
9. Toleikis, S. *et al*. Soft X-ray scattering using FEL radiation for probing near-solid density plasmas at few electron volt temperatures. *High Energy Density Phys.* **6,** 15–20 (2010).
10. Islam, M. N. *et al*. Femtosecond distributed soliton spectrum in fibers. *J. Opt. Soc. Am. B* **6,** 1149–1158 (1989).
11. Nakazawa, M., Kubota, H. & Tamura, K. Random evolution and coherence degradation of a high-order optical soliton train in the presence of noise. *Opt. Lett.* **24,** 318–320 (1999).
12. Thornhill, S. G. & ter Haar, D. Langmuir turbulence and modulational instability. *Phys. Rep.* **43,** 43–99 (1978).
13. Kivshar, Y. S. & Peyrard, M. Modulational instabilities in discrete lattices. *Phys. Rev. A* **46,** 3198–3205 (1992).
14. Strecker, K. E., Partridge, G. B., Truscott, A. G. & Hulet, R. G. Formation and propagation of matter-wave soliton trains. *Nature* **417,** 150–153 (2002).
15. Konotop, V. V. & Salerno, M. Modulational instability in Bose–Einstein condensates in optical lattices. *Phys. Rev. A* **65,** 021602 (2002).
16. Tai, K., Hasegawa, A. & Tomita, A. Observation of modulational instability in optical fibers. *Phys. Rev. Lett.* **56,** 135–138 (1986).
17. Kip, D., Soljacic, M., Segev, M., Eugeniev, E. & Christodoulides, D. N. Modulation instability and pattern formation in spatially incoherent light beams. *Science* **290,** 495–498 (2000).
18. Zakharov, V. E. & Ostrovsky, L. A. Modulation instability: the beginning. *Physica D* **238,** 540–548 (2009).
19. Kharif, C. & Pelinovsky, E. Physical mechanisms of the rogue wave phenomenon. *Eur. J. Mech. B* **22,** 603–634 (2003).
20. Onorato, M., Osborne, A. R., Serio, M. & Bertone, S. Freak waves in random oceanic sea states. *Phys. Rev. Lett.* **86,** 5831–5834 (2001).
21. Solli, D. R., Ropers, C., Koonath, P. & Jalali, B. Optical rogue waves. *Nature* **450,** 1054–1057 (2007).
22. Akhmediev, N. & Korneev, V. I. Modulation instability and periodic solutions of the nonlinear Schrodinger equation. *Theor. Math. Phys.* **69,** 1089–1093 (1986).
23. Van Simaeys, G., Emplit, P. & Haelterman, M. Experimental demonstration of the Fermi–Pasta–Ulam recurrence in a modulationally unstable optical wave. *Phys. Rev. Lett.* **87,** 033902 (2001).
24. Dudley, J. M., Genty, G., Dias, F., Kibler, B. & Akhmediev, N. Modulation instability, Akhmediev breathers and continuous wave supercontinuum generation. *Opt. Express* **17,** 21497–21508 (2009).
25. Kibler, B. *et al*. The Peregrine soliton in nonlinear fibre optics. *Nature Photon.* **6,** 790–795 (2010).
26. Nakazawa, M., Suzuki, K., Kubota, H. & Haus, H. A. Higher-order solitons and modulational instability. *Phys. Rev. A* **39,** 5768–5776 (1989).
27. Kutz, J. N., Lyngå, C. & Eggleton, B. J. Enhanced supercontinuum generation through dispersion-management. *Opt. Express* **13,** 3989–3998 (2005).
28. Solli, D. R., Ropers, C. & Jalali, B. Active control of rogue waves for stimulated supercontinuum generation. *Phys. Rev. Lett.* **101,** 233902 (2008).
29. Solli, D. R., Jalali, B. & Ropers, C. Seeded supercontinuum generation with optical parametric down-conversion. *Phys. Rev. Lett.* **105,** 233902 (2010).
30. Solli, D. R., Ropers, C. & Jalali, B. Rare frustration of optical supercontinuum generation. *Appl. Phys. Lett.* **96,** 151108 (2010).
31. Kelkar, P. V., Coppinger, F., Bhushan, A. S. & Jalali, B. Time-domain optical sensing. *Electron. Lett.* **35,** 1661–1662 (1999).
32. Mussot, A. *et al*. Spectral broadening of a partially coherent CW laser beam in single-mode optical fibers. *Opt. Express* **12,** 2838–2843 (2004).
33. Droques, M. *et al*. Symmetry-breaking dynamics of the modulational instability spectrum. *Opt. Lett.* **36,** 1359–1361 (2011).
34. Intonti, F. *et al*. Quantum mechanical repulsion of exciton levels in a disordered quantum well. *Phys. Rev. Lett.* **87,** 076801 (2001).
35. Garay-Palmett, K. *et al*. Photon pair-state preparation with tailored spectral properties by spontaneous four-wave mixing in photonic-crystal fiber. *Opt. Express* **15,** 14870–14886 (2007).
36. Solli, D. R., Gupta, S. & Jalali, B. Optical phase recovery in the dispersive Fourier transform. *Appl. Phys. Lett.* **95,** 231108 (2009).

Acknowledgements

This work was supported by the National Science Foundation including CIAN ERC, the Defense Advanced Research Project Agency (DARPA/DSO) Physical Intelligence programme and the Deutsche Forschungsgemeinschaft (DFG-ZUK 45/1). D.R.S. thanks B. de La Brea for helpful discussions.

Author contributions

All authors were closely involved in this study and contributed to the ideas, realization of the experiments, data analysis and interpretation, and writing of the paper.

Additional information

The authors declare no competing financial interests. Supplementary information accompanies this paper at www.nature.com/naturephotonics. Reprints and permission information is available online at http://www.nature.com/reprints. Correspondence and requests for materials should be addressed to D.R.S.